Clay Minerals, (2015) **50**, 41–54

Structural study of Zn-exchanged natural clinoptilolite using powder XRD and positron annihilation data

L. T. DIMOWA[1],* O. E. PETROV[1], N. I. DJOURELOV[2] AND B. L. SHIVACHEV[1]

[1] *Institute of Mineralogy and Crystallography, Bulgarian Academy of Sciences, Acad. G. Bonchev Street, Block 107, 1113 Sofia, Bulgaria, and* [2] *Institute for Nuclear Research and Nuclear Energy, Bulgarian Academy of Sciences, 72 Tzarigradsko Chaussee Blvd., BG-1784 Sofia, Bulgaria*

(*Received 25 July 2014; revised 29 January 2015; Guest Editor: A. Langella*)

ABSTRACT: Zn-exchanged natural clinoptilolite was studied by powder X-ray diffraction and positron annihilation lifetime spectroscopy. The original clinoptilolite tuff was subjected to size fractionation by sedimentation and dissolution of cristobalite (opal-C). After Zn^{2+}-exchange the purified clinoptilolite sample contained 2.2 Zn^{2+} ions per unit cell. Structural details obtained by Rietveld refinement showed that the Zn^{2+} cations are located in three sites (Zn1, Zn2 and Zn3) in the channels of the clinoptilolite. Site Zn1 is located in the centre of channel-A (Mg^{2+}-M4 site). Site Zn2 is in channel-B, next to the calcium M2 position. A new Zn3 site is located in channel-A, in imminent proximity to Zn1. Positron Annihilation Lifetime Spectroscopy (PALS) was employed to assess the Zn exchange. As the cation content influences the free volume of the channels, the ion-exchange process can be monitored by PALS. The results suggest the existence of two sizes of cavities, in accordance with the structural refinement.

KEYWORDS: clinoptilolite, Zn exchange, XRD, Rietveld, positron annihilation lifetime spectroscopy.

Natural zeolites have been investigated intensively because of their ion exchange, molecular sieve, catalytic and adsorption properties (Colella, 1999). Their unique microporous structure can be subdivided into three relatively independent building entities: aluminosilicate framework, cations balancing the charge deficit and water molecules. The framework consists of interconnecting SiO_4 and AlO_4 tetrahedra to produce tetrahedral rings. The cations and water molecules occupy the zeolite channels and ion exchange and dehydration-rehydration processes are possible, thus providing possibilities for targeted modification of zeolites.

* E-mail: Louiza.Dimova@gmail.com
DOI: 10.1180/claymin.2015.050.1.05

To date, >50 natural zeolites have been discovered and investigated. However, only eight species of zeolite have deposits large enough for industrial exploitation, namely analcime, chabazite, clinoptilolite-heulandite, mordenite, erionite, ferrierite, laumontite and phillite. One of the deposits exploited for clinoptilolite is Beli Plast, East Rhodopes, Bulgaria. Clinoptilolite has a wide range of applications in environmental protection, chemistry and other industries because it is stable up to ~550–600ºC and remains unaffected over a wide pH range (Mumpton, 1960; Boles, 1972; Ming & Mumpton, 1989).

The antibacterial activity of natural zeolites (especially of clinoptilolite) after ion exchange with heavy metals such as Zn^{2+}, Cu^{2+} and Ag^{+} cations is well established. Several clinoptilolite formulations have been used for treating different

bacterial infections and suppressing bacterial strains (Hrenovic *et al.*, 2013). Recently, this antibacterial activity has been employed in dermatology and cosmetics (Korkuna *et al.*, 2006; Copcia *et al.*, 2013). In medical formulations, clinoptilolite may act not only as a carrier of zinc ions, but may also be employed as a "buffer" for prolonged and more gradual release of Zn (Habbema *et al.*, 1989; Holland *et al.*, 1992; Kirov & Terziyski, 1997; Cerri *et al.*, 2004). Thus, in-depth characterization and structural investigation of the ion exchange, selectivity, specificity and structural characteristics of natural zeolites (site occupancies, pH dependency, thermal stability, etc.) are important for the design and modification of zeolites for targeting specific properties. The structural investigations are carried out mainly by X-ray diffraction (XRD) techniques, which provide information on the long-range atomic order. The most powerful method is based on investigation of single crystals. However, the industrially important natural zeolites are usually tuffs (microcrystalline), making powder diffraction techniques essential for such studies. Structure determination from powder data has become informative mainly due to the application of the Rietveld approach (Rietveld 1967, 1969).

Previous single-crystal studies have shown that the Zn^{2+} exchange of clinoptilolite is not complete (0.33 atoms per unit cell) (Dimowa *et al.* 2011). Garsia-Basabe *et al.* (2012) studied Co^{2+}-, Ni^{2+}-, Cu^{2+}- and Zn^{2+}-exchanged natural and de-aluminated clinoptilolite and proposed two positions for zinc, one with low occupancy. However, the positions of Zn^{2+} in the channels was not reported in detail. Dimowa *et al.* (2013) studied Zn-exchanged clinoptilolite, treated thermally at 300ºC and 500ºC, to locate the Zn cations in the channels without the presence of water.

The purpose of the present investigation was to achieve maximum ion exchange of Zn^{2+} ions into a clinoptilolite sample starting from an aqueous solution of $ZnCl_2$ and to characterize the resulting Zn-exchanged clinoptilolite by powder XRD and positron annihilation lifetime spectroscopy (PALS).

EXPERIMENTAL

Materials

The clinoptilolite-rich tuff (Ct, 80 wt.%, according to quantitative XRD analysis) from the Beli Plast deposit, Eastern Rhodope, Bulgaria was purified to >98 wt.% clinoptilolite by crushing, passing through a 0.16 mm mesh sieve and fractionation by timed sedimentation into four fractions: 0.160–0.032 mm, 0.032–0.016 mm, 0.016 and >0.002 mm in water. The additional mineral phases (denser than clinoptilolite) present in the 0.032–0.016 mm size fraction, which is richer in clinoptilolite, were removed by heavy liquid separation (bromoform-ethanol solution with a density of 2.2 g cm^{-3}). The sample was centrifuged at 4000 rpm for 10 min and the clinoptilolite material obtained, which contained a small amount of cristobalite (opal-C), was labelled as Co-c. The Co-c material was purified further by dissolution of SiO_2 as follows: Co-c (100 mg) was heated to boiling in NaOH solution (0.5 L, 0.5 mol dm^{-3}) for 7 mins. The hot suspension was filtered, washed with distilled water until pH ~6.5–7 and dried at room temperature. This purified clinoptilolite sample was labelled as Cp.

Zinc exchange

Cp (1 g) was suspended in $ZnCl_2$ solution (15 mL, 1 M), placed in a Teflon autoclave and heated at 100ºC for 16 days. The autoclave was shaken every day and the $ZnCl_2$ solution was renewed every second day. Before renewal of the $ZnCl_2$, the solution was adjusted to pH >4.7. The Zn-exchanged material was filtered, washed with distilled water (5 × 300 mL) and dried at room temperature. This Zn-exchanged clinoptilolite was labelled as Czn.

Characterization

Powder X-ray diffraction (XRD) data were collected at room temperature on a Bruker D2 Phaser diffractometer (Ni-filtered Cu$K\alpha$ radiation, 30 kV, 10 mA), in the range 8–50º2θ, using a step size of 0.05º2θ and counting time of 1 s per step. The powder patterns designated for subsequent Rietveld refinement were collected on a Bruker D8 Advance diffractometer (Cu$K\alpha$ radiation, 40 kV, 40 mA) in the range 5 to 100º2θ, using a step size of 0.02º and a collection time of 10 s per step. Standard sample holders with 0.5 mm depth were used.

The Rietveld method (Rietveld, 1967, 1969) was applied for structural refinement of samples Cp and Czn. The unit-cell parameters and all atomic coordinates were refined using the *TOPAS*©

https://doi.org/10.1180/claymin.2015.050.1.05 Published online by Cambridge University Press

software (*Topas* V4.2, 2004). The background was fitted by a Chebyshev polynomial with 20 coefficients and the pseudo-Voigt peak function was applied for peak modelling. The refinement was conducted with the clinoptilolite structural model of Koyama & Takeuchi (1977).

The chemical composition of Cp and Czn was obtained by Inductively Coupled Plasma optical emission spectroscopy (ISP-OES) on a Varian Vista MPX CCD, while the Zn content during ion exchange was measured by Atomic Absorption Spectroscopy (AAS) on a Perkin Elmer 3030 apparatus. Fourier Transform Infrared Spectroscopy (FTIR) was used to complement the XRD results of sample Co-c and to compare samples Cp and Czn. The transmission FTIR spectra transmission spectra were obtained from KBr pellets using a TENSOR 37 Bruker FTIR spectrometer. Differential Thermal Analysis and Thermo Gravimetry (DTA-TG) curves in the 30−750ºC temperature range were obtained from ground Cp and Czn (sample weight 12±0.2 mg) under a heating rate of 10ºC/min and an air flow of 50 mL/min on a Stanton Redcroft apparatus.

Positron annihilation lifetime spectroscopy (PALS)

The PALS spectrometer was a fast coincidence system with a prompt resolution Gaussian curve of 240 ps (FWHM). The spectra were recorded in 8192 channels with 12.4 ps width. A ^{22}NaCl positron source with activity of ~30 μCi, sealed between two Kapton foils of 7.5 μm thickness was used in sandwich geometry between two identical samples. The measurements were performed in air at room temperature. The recorded lifetime spectra contained 3×10^6 counts. The analysis of the spectra, cut 10 ns left and 30 ns right from zero time, was performed with the *LT v.9.2* program (Kansy, 1996). The spectral analysis showed good fitting (variance of the fit ~1.1) with four exponential components. The lifetimes of the components were within the ranges: τ_1 = 0.12−0.18 ns; τ_2 = 0.40−0.44 ns, $\tau_3 \approx$ 1.5 ns, and τ_4 = 3.7−5.6 ns. The allocation of components for this type of analysis was as follows: τ_4 and τ_3 are due to pick-off annihilation of *ortho*-Positronium (*o*-Ps) localized into pores (bigger and smaller in size), τ_2 is the lifetime of the positrons (e^+) not forming Ps, and τ_1 is due to *para*-Ps annihilation.

Coincidence doppler broadening spectroscopy (CDBS)

The CDBS system used was set up according to Van Petegem *et al.* (2003). It consisted of two Ortec HPGe detectors each with 14% efficiency and a resolution of 1.2 keV for the 514 keV line of ^{85}Sr. The detectors were facing each other at a distance of 0.30 m, with the source sample sandwiched in the middle. Their signals were read by Ortec 572 amplifiers, the unipolar signals of which fed two Silena 7423UHS Analogue-to-Digital-Converters (ADCs) communicating with a PCI6533 NI card driven by *Labview* software. The system allowed a count rate of 250 s^{-1} for a source of 50 mCi activity and showed a resolution of G = 0.9 keV. The statistics in the extracted coincidence diagonal cut from the coincidence matrix was ~1.2×10^7 counts.

RESULTS AND DISCUSSION

Chemical analyses of Ct, Co-c, Cp and Czn clinoptilolite samples

The chemical analyses of the Ct, Co-c, Cp and Czn samples are listed in Table 1. The purified sample Co-c has a larger LOI and smaller oxide contents compared to the Ct. For CaO the weight loss exceeds 1 wt.%; for SiO_2, K_2O and Fe_2O_3 it is 0.5−0.8 wt.%, and for the remaining oxides it is <0.3 wt.%. The opal-C removal in sample Cp was

TABLE 1. Chemical composition (wt.%) of the analysed samples Ct, Co-c, Cp and Czn.

Oxide	Ct	Co-c	Cp	Czn
SiO_2	69.46	68.65	66.10	64.75
Al_2O_3	10.91	10.81	12.08	11.74
Fe_2O_3	0.87	0.19	0.28	0.31
CaO	4.77	3.60	3.45	0.80
Na_2O	0.36	0.27	1.16	0.21
K_2O	2.72	2.00	1.92	0.70
MgO	0.93	0.71	0.72	0.29
TiO_2	0.11	0.08	0.05	0.06
MnO	0.16	0.02	0.01	0.01
ZnO	<LOD*	<LOD*	<LOD*	6.59
LOI**	9.63	13.55	14.20	14.56
Total	99.92	99.88	99.97	100.02

* LOD = limit of detection, 0.01 for Zn
** LOI = loss on ignition

https://doi.org/10.1180/claymin.2015.050.1.05 Published online by Cambridge University Press

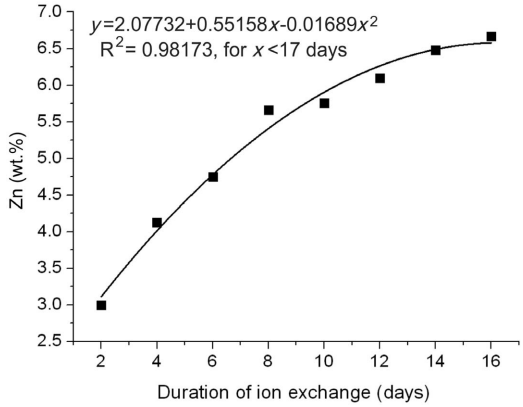

FIG. 1. Zn-content of sample Czn during Zn-exchange.

confirmed by the decrease in SiO_2 (~2.5 wt.%) compared to Co-c. The calculated Si/Al ratios were 5.38 and 4.62 for Co-c and Cp, respectively. Interestingly, in sample Cp the Na content increased to 1.16 wt.% from 0.27 wt.% in Co-c, probably due to partial exchange with Na^+ during the chemical treatment. The decrease of Ca and K in sample Cp is in agreement with Na^+-exchange.

During Zn-exchange, the Zn content of the samples was monitored by AAS (Fig. 1). The Zn-content increased from 0.002 to 3.00 wt.% over the first two days and to 5.66 wt.% by the 8th day. Thus, the rate of Zn^{2+} ion exchange was faster during the first 2 days (1.5 wt.% per day), decreasing to ~0.45 wt.% per day between the 2nd and 8th day and to ~0.125 wt.% per day after the 8th day. The Zn^{2+} content of the Czn sample after 16 days of exchange was 6.67 wt.%.

The structural formulae of the Cp and Czn samples obtained from the chemical analyses (Table 1) were calculated on the basis of 72 oxygen atoms per unit cell and are shown below:

$$\text{Cp } (Na_{1.01}Ca_{1.66}K_{1.10}Mg_{0.48})\ Al_{6.39}Si_{29.52}O_{72}\ 21.20H_2O \quad (1)$$

$$\text{Czn } (Na_{0.19}Ca_{0.39}K_{0.40}Mg_{0.20}Zn_{2.23})\ Al_{6.31}Si_{29.61}O_{72}\ 22.20H_2O \quad (2)$$

The contents of the original K^+, Na^+, Ca^{2+} and Mg^{2+} cations in sample Czn are very low. By contrast the number of water molecules increased by one molecule per unit cell compared to Cp.

During the ion exchange, the pH levels of the solutions varied between 4.5 and 5. The calculated Si/Al ratio for Cp is almost identical to Czn (4.62 and 4.69, respectively), suggesting that the aluminosilicate framework was not affected during ion exchange.

Powder XRD analyses for Ct, Co-c, Cp and Czn clinoptilolite samples

The XRD analysis of sample Ct shows the presence of cristobalite (opal-C), quartz, plagioclase, K-feldspar, calcite, dolomite and mica (Fig. 2). These minerals were removed successfully by purification. All impurities except opal-C were removed by heavy-liquid separation. The subsequent chemical procedure (with NaOH solution) was applied to remove opal-C. The resulting diffraction patterns for different boiling times (minutes) with NaOH are shown in Fig. 3.

In order to preserve the clinoptilolite structure a precise estimation of the optimum boiling time was necessary. For this purpose, the XRD traces of the sample were recorded every minute throughout the boiling time (2–15 min). Opal-C is visible in the XRD pattern (peak at ~21.5º2θ) of samples that were boiled for up to 7 min. The intensities of the clinoptilolite peaks remain virtually unchanged up to the 9th minute. For longer boiling times and especially after the 12th minute, significant changes appeared in the powder patterns indicating dissolution of the aluminosilicate framework (Fig. 3). Therefore, 7 min was considered optimum boiling time for opal-C removal.

FTIR analyses of Co-C, Cp and Czn samples

The FTIR spectra of the Co-c, Cp and Czn samples are similar (Fig. 4). The intense bands are located in the range 400–1200 cm^{-1} and are attributed to vibrations of the Al/SiO_4 tetrahedra.

The band at 465 cm^{-1} is due to the internal bending of the Al/SiO_4 tetrahedra and thus cannot be related to the degree of crystal order of the clinoptilolite framework. On the other hand, the band at 605 cm^{-1}, due to double-ring stretching is indicative of the clinoptilolite structure. Thus, the ratio of intensities of the bands (465 and 605 cm^{-1}) shows the degree of crystal order of the clinoptilolite (Perraki & Orfanoudaki, 2004; Elaiopoulos *et al.*, 2008). Comparing the samples Co-c and Cp, the ratio remains constant. The IR data suggest that the structure of Cp is not affected by the chemical treatment with NaOH, in accordance with the XRD analysis. The band at 794 cm^{-1} is assigned to the external tetrahedral

https://doi.org/10.1180/claymin.2015.050.1.05 Published online by Cambridge University Press

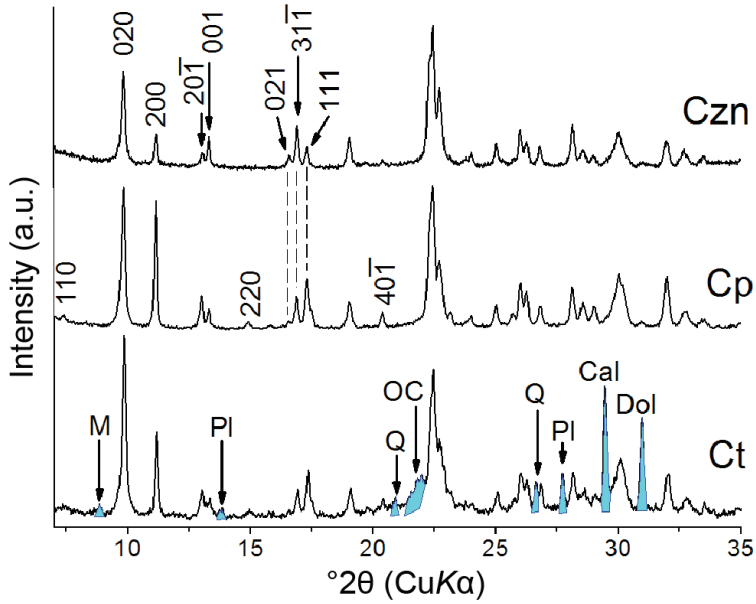

FIG. 2. XRD patterns of Ct, Cp and Czn. M = mica, Pl = plagioclase, Q = quartz, OC = opal-C, Cal = calcite, Dol = dolomite.

vibrations and is attributed to clinoptilolite, quartz, cristobalite, opal and amorphous silica (Hernández-Ortiz *et al.*, 2012). Therefore, the greater intensity of the 794 cm^{-1} band, with respect to those at 605

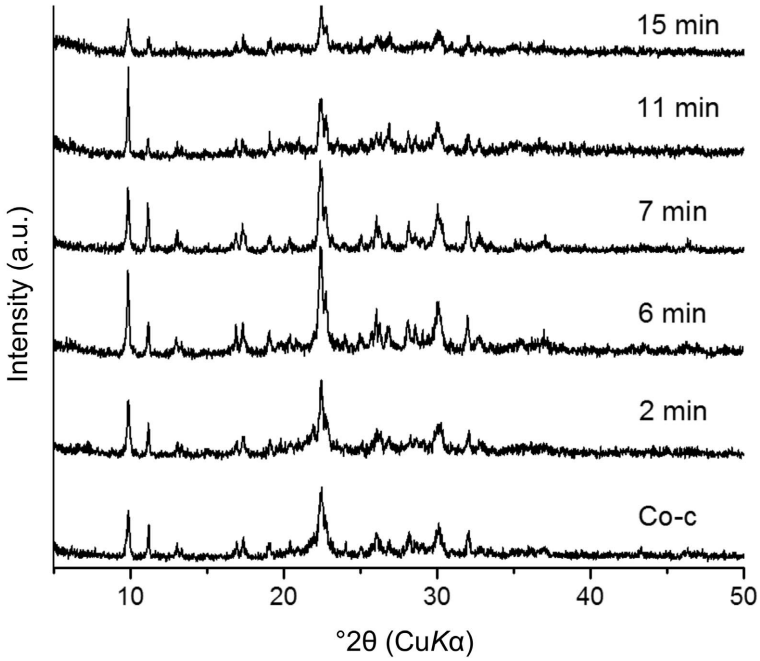

FIG. 3. Powder XRD patterns of Co-c after boiling with NaOH for different periods of time. The main diffraction maxima of opal-C are at ~22 and ~37°2θ.

https://doi.org/10.1180/claymin.2015.050.1.05 Published online by Cambridge University Press

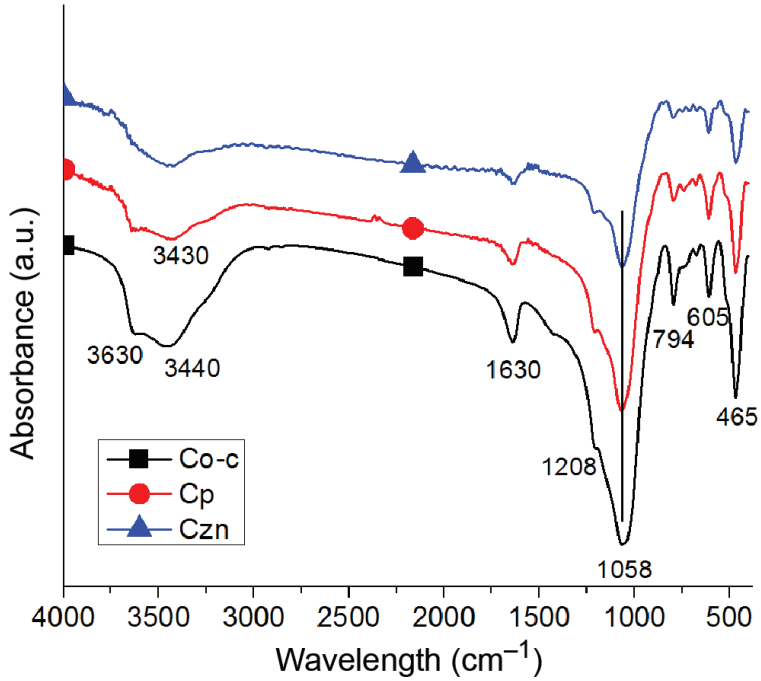

FIG. 4. FTIR spectra of samples Co-c, Cp and Czn.

and 465 cm^{-1} in Co-c compared to Cp and Czn, is indicative of the presence of opal-C in the former (Bertaux *et al.*, 1998; Moirou *et al.*, 2000).

The most intense band in all of the samples is observed at 1058 cm^{-1} and is due to external tetrahedral Si–O–Si and Si–O–Al linkages. According to the number of Al atoms in the clinoptilolite framework, the position of this band varies between 1090 and 1048 cm^{-1} (Rodríguez-Iznaga *et al.*, 2002; Elaiopoulos *et al.*, 2008). This band shifts towards lower wavenumbers as the Al content in the structure increases. Therefore, dealumination causes a shift of this band to higher wavenumbers (Mozgawa, 2000). For Co-c, Cp and Czn samples, the position of this band remains unchanged and suggests a constant Al content. The shoulder of the band at 1208 cm^{-1} is related to the internal tetrahedral asymmetric stretching (Rodriguez-Fuentes *et al.*, 1998).

The bands associated with vibrations of water molecules and OH groups are visible in the range 1600–3700 cm^{-1}. The band at 1630 cm^{-1} is assigned to the H_2O bending modes. The band at 3440 cm^{-1} is assigned to the asymmetric stretching mode of intermolecular hydrogen bonding. The band at ~3600 cm^{-1} is related to the stretching mode of H–O–H (Castaldi *et al.*, 2005). The band at 3620 cm^{-1} is related to intermolecular hydrogen bonding and OH from Si–OH–Al bridges (Doula *et al.*, 2002; Korkuna *et al.*, 2006). Finally, a small band at 3630 cm^{-1} is visible in samples Co-c and Cp, but not in Czn. This feature might be due to the different water arrangement around Zn^{2+}.

DTA TG analyses for purified and exchanged clinoptilolite samples

The DTA data (Fig. 5) suggest that the Cp and Czn samples have thermal behaviour typical of clinoptilolite with a broad endothermic peak between 25 and ~350ºC (Mumpton, 1960; Alietti *et al.*, 1975), corresponding to release of H_2O molecules from the channels. The maximum of the endothermic effect is around 105–110ºC for the Cp sample. In Czn this maximum is ~90ºC, probably due to the tighter coordination of H_2O molecules to the Zn cations allowing larger quantities of loosely bound water into the channels. In the TG curves the mass loss up to 750ºC, related to dehydration, is 14.2 and 14.6% for Cp and Czn, respectively. On the basis of the above-mentioned results, it is inferred that the clinoptilolite Czn studied was

https://doi.org/10.1180/claymin.2015.050.1.05 Published online by Cambridge University Press

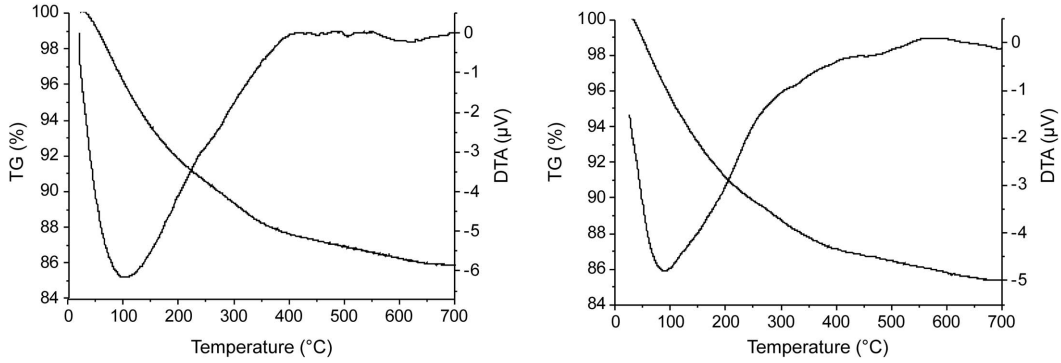

FIG. 5. DTA-TG diagram of Cp (left) and Czn (right).

almost fully exchanged with Zn cations and is suitable for detailed structural analysis by the Rietveld method.

Rietveld refinement of samples Cp and Czn

The initial stages of the refinement showed that there is a slight intensity excess at ~22º2θ, which corresponds to the presence of residual opal-C. Adding cristobalite as a second phase in the refinement process improved the profile fit yielding 1.65 wt. % cristobalite. The structural refinement of clinoptilolite in samples Cp and Czn was performed in several consecutive stages. The first stage of refinement used the positions of framework atoms based on the model of Koyama & Takeuchi (1977). During the initial stage of the refinement, the framework atomic coordinates were kept fixed, while the occupancies of the cationic positions were adjusted using the chemical data and allowed to refine. Then, the H_2O sites were located and their coordinates and occupancies were refined. In the next step, the cations and H_2O positions and occupancies were fixed and the framework coordinates were relaxed (refined). In the final cycle of the structure refinement, the cations and H_2O were also relaxed. Reliability factors and a difference plot showed good agreement between the experimental data and the refined model (Table 2).

After the initial refinement cycles, R_{wp} values reached 18%. The refinement of the occupancies of the cationic sites decreased R_{wp} to 12%. The

TABLE 2. Crystal system, space group, agreement factors (%), phases present and unit-cell parameters for purified clinoptilolite samples Cp and Czn.

Sample	Cp	Czn
Crystal system	Monoclinic	Monoclinic
Space group	*C*2/*m*	*C*2/*m*
R_{exp}	3.47	2.95
R_{wp}	7.55	5.47
R_p	5.64	4.22
GOF	2.26	1.85
DW	0.51	0.70
R_B	1.83	1.66
Phase 1 clinoptilolite wt.%	98.35	98.35
Phase 2 cristobalite low wt.%	1.65	1.65
a (Å)	17.669(2)	17.649(2)
b (Å)	17.9382)	17.964(2)
c (Å)	7.409(2)	7.405(2)
β (º)	116.33(3)	116.24(3)
V (Å^3)	2104(4)	2106(4)

https://doi.org/10.1180/claymin.2015.050.1.05 Published online by Cambridge University Press

coordinates of the cationic positions changed slightly and R_{wp} further decreased to 10.5% (with improved difference plot). The addition of H_2O molecules improved R_{wp} to 9%. The last stages of the refinement of framework, cationic and H_2O sites yielded a R_{wp} of 7.5% and showed good agreement with the chemical data (Fig. 6). The same refinement scheme was applied for sample Czn, which showed a final R_{wp} of 5.8% (Fig. 6).

The sites, Wyckoff positions, atomic coordinates, occupancies and isotropic displacement parameters for sample Czn are listed in Table 3.

Structure description and crystal-chemical features for Cp

Sample Cp shows no significant structural changes compared to the starting structural model of Koyama & Takeuchi (1977). The typical cationic positions in the channels were preserved: Na^+ (M1), Ca^{2+} (M2), K^+ (M3) and Mg^{2+} (M4) as well as the positions of the H_2O molecules. The cation positions 1, 2, 3 and 4 are occupied by Na^+ (1.04), Ca^{2+} (1.76), K^+ (1.12) and Mg^{2+} (0.52) cations per unit cell, respectively. Seven H_2O molecules were located and produced a total amount of 20.2 H_2O molecules per unit cell. The overall results are in good agreement with the chemical analysis data.

Structure description and crystal-chemical features of Czn

Three cationic positions were located in the channels of sample Czn, namely Zn1, Zn2 and Zn3 numbered in reducing occupancy order (Fig. 7).

Position Zn1 is identical to the magnesium position M4 and is occupied by one Zn ion per unit cell (the possible maximum is two atoms). Six H_2O molecules in three positions at appropriate distances (O15(×2), O16(×2) and O17(×2)), coordinate in an octahedral arrangement around the position Zn1 (Fig. 7) (Table 4).

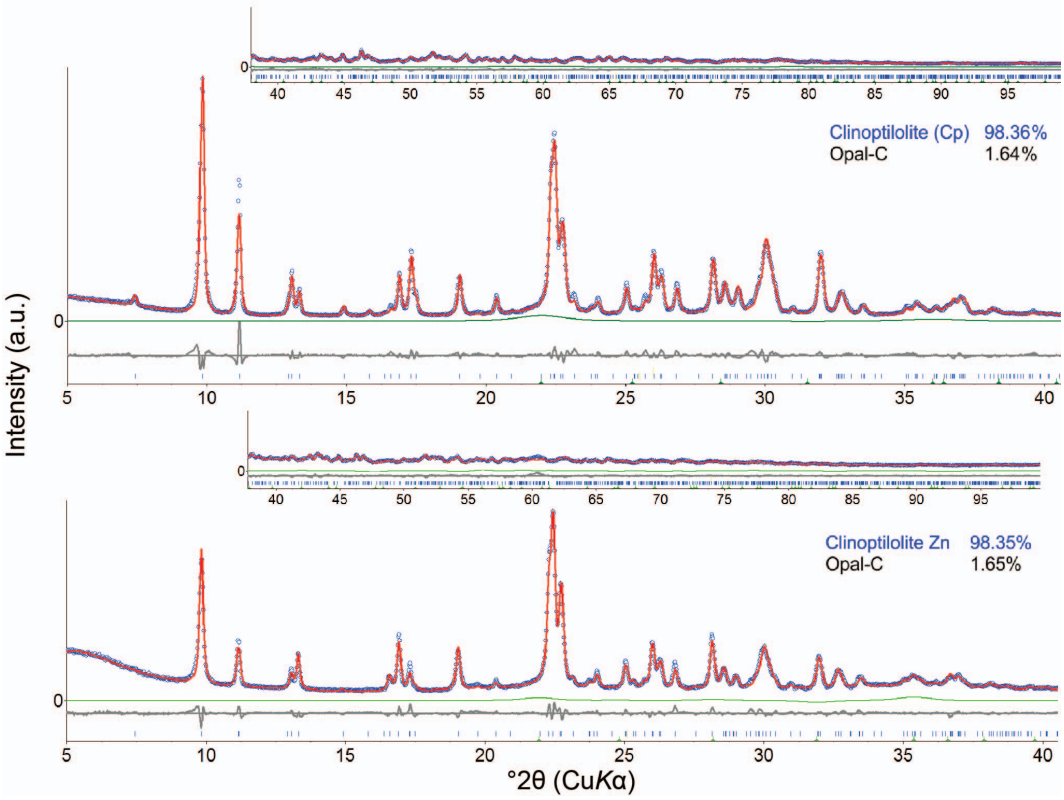

FIG. 6. Rietveld full-profile fit of the Cp and Czn samples. The main diffraction maxima of opal-C are at ~22 and ~37°2θ.

https://doi.org/10.1180/claymin.2015.050.1.05 Published online by Cambridge University Press

TABLE 3. Sites, Wyckoff positions, atomic coordinates, occupancies and isotropic displacement parameters of sample Czn. Positions T(1, 2, 3, 4 and 5) refer to simultaneous occupancy of Si and Al.

Site		Wp	*x*	*y*	*z*	Atom	Occ.
Biso							
T1	8j	0.179(3)	0.168(2)	0.094(4)	Si^{4+}	1	1.5(3)
T2	8j	0.212(3)	0.412(4)	0.503(3)	Si^{4+}	1	1.5(3)
T3	8j	0.208(2)	0.191(2)	0.714(3)	Si^{4+}	1	1.5(3)
T4	8j	0.068(4)	0.299(3)	0.413(4)	Si^{4+}	1	1.5(3)
T5	4g	0	0.219(2)	0	Si^{4+}	1	1.5(3)
O1	4i	0.201(2)	0.5	0.462(2)	O^{2-}	1	1.7(3)
O2	8j	0.232(2)	0.122(2)	0.611(3)	O^{2-}	1	1.8(6)
O3	8j	0.184(4)	0.156(2)	0.880(3)	O^{2-}	1	1.6(4)
O4	8j	0.231(3)	0.103(3)	0.246(3)	O^{2-}	1	1.8(4)
O5	4h	0	0.318(2)	0.5	O^{2-}	1	1.5(3)
O6	8j	0.082(2)	0.168(4)	0.050(3)	O^{2-}	1	1.8(9)
O7	8j	0.123(3)	0.230(3)	0.544(2)	O^{2-}	1	1.8(4)
O8	8j	0.012(2)	0.273(3)	0.183(3)	O^{2-}	1	1.8(5)
O9	8j	0.214(3)	0.251(2)	0.192(2)	O^{2-}	1	1.8(4)
O10	8j	0.116(4)	0.377(6)	0.420(2)	O^{2-}	1	1.8(4)
O11	4i	0.234(5)	0.5	0.035(3)	O^{2-}	0.50(2)	2.3(5)
O12	4i	0.038(4)	0	0.718(2)	O^{2-}	0.35(3)	2.4(5)
O13	8j	0.076(5)	0.438(4)	0.941(5)	O^{2-}	0.89(6)	2.3(4)
O14	2d	0	0.5	0.5	O^{2-}	0.35(3)	2.3(5)
O15	4h	0	0.116(5)	0.5	O^{2-}	0.34(3)	1.7(6)
O16	4i	0.045(3)	0	0.232(4)	O^{2-}	0.64(6)	2.3(5)
O17	4i	0.136(3)	0	0.723(3)	O^{2-}	0.52(2)	1.9(3)
Zn1	2c	0	0	0.5	Zn^{2+}	0.5(1)	1.5(6)
Zn2	4i	0.044(3)	0.5	0.270(4)	Zn^{2+}	0.17(3)	2.4(5)
Zn3	4i	0.092(4)	0	0.464(3)	Zn^{2+}	0.13(2)	2.1(7)

Attempts to locate more than one zinc ion in position Zn1 were not successful. Position Zn2 takes 0.68 Zn ions and is similar to the position M2 in channel B. In the initial form (Cp) this position is occupied by Ca^{2+}. Zinc ions shifted this position slightly along the *a* and *c* axes away from the channel centre. Zinc cations (Zn2) are coordinated by two H_2O positions (O13 and O14, Table 4). Two framework oxygen atoms (O1 and O10) also help to complete Zn2 coordination.

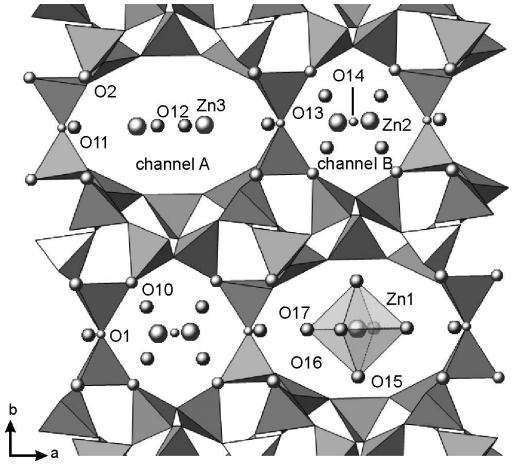

FIG. 7. Positions of cations and water molecules in sample Czn.

The refinement of the occupancies for Zn1 and Zn2 positions yielded 1.68 zinc atoms per unit cell; however, chemical data showed 2.19 zinc atoms per unit cell. The missing 0.52 Zn ions were located in a third position situated on the mirror plane in the channel A designated as Zn3. Actually, this position is analogous to M1 but is shifted towards the centre of the A channel. Therefore, the distance between the Zn3 and Zn3′ positions is 1.7 Å and their simultaneous occupation is forbidden. Position Zn3 is also close to Zn1 with a Zn1–Zn3 distance of 1.4 Å. The H_2O at position O12 coordinates Zn3 specifically (distance 2.45 Å). The total amount of O12 is 1.4 molecules per unit cell. Water O11 and

https://doi.org/10.1180/claymin.2015.050.1.05 Published online by Cambridge University Press

TABLE 4. Selected atomic bond distances of samples Cp and Czn.

Cp				Czn			
Atom1	Atom2	No	*d* (Å)	Atom1	Atom2	No	*d* (Å)
Framework cations							
T1	O4	1 ×	1.604(33)	T1	O6	1 ×	1.601(25)
	O6	1 ×	1.623(25)		O4	1 ×	1.610(22)
	O9	1 ×	1.634(32)		O3	1 ×	1.639(23)
	O3	1 ×	1.644(26)		O9	1 ×	1.651(25)
T2	O1	1 ×	1.625(31)	T2	O1	1 ×	1.600(40)
	O2	1 ×	1.657(35)		O10	1 ×	1.662(34)
	O4	1 ×	1.677(25)		O2	1 ×	1.678(31)
	O10	1 ×	1.682(35)		O4	1 ×	1.700(20)
T3	O2	1 ×	1.605(28)	T3	O2	1 ×	1.602(28)
	O3	1 ×	1.607(28)		O3	1 ×	1.603(24)
	O9	1 ×	1.613(24)		O9	1 ×	1.607(24)
	O7	1 ×	1.617(25)		O7	1 ×	1.637(15)
T4	O10	1 ×	1.593(21)	4	O10	1 ×	1.601(20)
	O5	1 ×	1.605(25)		O7	1 ×	1.612(17)
	O7	1 ×	1.607(22)		O8	1 ×	1.622(19)
	O8	1 ×	1.621(28)		O5	1 ×	1.633(18)
T5	O8	2 ×	1.609(28)	T5	O8	2 ×	1.604(19)
	O6	2 ×	1.609(25)		O6	2 ×	1.610(19)
Exchangable cations							
Na	O17	1 ×	1.287*(32)	Zn1	O12	2 ×	1.450*(51)
	K	1 ×	1.913*(43)		Zn3	2 ×	1.759*(67)
	Mg	1 ×	2.267(33)		O15	2 ×	2.080(88)
	O12	1 ×	2.387(53)		O17	2 ×	2.239(78)
	O11	1 ×	2.601(44)		O16	2 ×	2.444(58)
	O16	1 ×	2.653(54)	Zn2	O14	1 ×	2.160(40)
	O2	2 ×	2.821(43)		O13	2 ×	2.295(25)
	O15	2 ×	3.053(43)		O1	1 ×	2.496(22)
	O3	2 ×	3.138(54)		O10	2 ×	2.548(21)
Ca	O13	2 ×	2.3695(53)		O13	2 ×	2.960(53)
	O14	1 ×	2.548(34)	Zn3	O16	1 ×	1.539*(59)
	O1	1 ×	2.593(43)		O17	1 ×	1.720*(88)
	O13	2 ×	2.636(63)		O12	1 ×	2.091(73)
	O10	2 ×	2.761(53)		O12	1 ×	2.454(89)
K	O11	1 ×	0.690*(48)		O15	2 ×	2.724(68)
	O17	1 ×	2.349(39)		O2	2 ×	3.123(19)
	O12	1 ×	2.823(38)				
	O3	2 ×	2.960(53)				
	O2	2 ×	3.059(42)				
	O13	2 ×	3.186(44)				
Mg	O17	2 ×	1.902*(4)				
	O15	2 ×	2.044(3)				
	O12	2 ×	2.607(4)				
	O16	2 ×	2.682(3)				

the framework oxygen O2 are too far away from Zn3 (>3 Å) to be described as 'coordinating'. The Rietveld refinement yielded 3.6H_2O molecules less than the chemical formula. Some H_2O molecules (positions) with low occupancies probably could not be located by the XRD data.

https://doi.org/10.1180/claymin.2015.050.1.05 Published online by Cambridge University Press

TABLE 4 (*contd.*)

Cp				Czn			
Atom1	Atom2	No	*d* (Å)	Atom1	Atom2	No	*d* (Å)
H_2O molecules							
O11	O13	2 ×	2.737(48)	O11	O17	1 ×	2.193*(70)
	O17	1 ×	2.977(64)		O13	2 ×	2.788(13)
	O4	2 ×	3.041(63)		O4	2 ×	3.039(22)
O12	O17	1 ×	1.149*(73)		O3	2 ×	3.091(19)
	O16	1 ×	2.551(64)	O12	O16	1 ×	1.67*(12)
	O16	1 ×	2.775(55)		O17	1 ×	1.72*(11)
	O6	2 ×	3.156(51)		O15	2 ×	2.536(87)
O13	O11	1 ×	2.737(58)		O12	1 ×	2.900(10)
	O13	1 ×	2.873(62)	O13	O13	1 ×	2.241(43)
	O13	1 ×	3.054(49)		O14	1 ×	3.138(22)
	O8	1 ×	3.091(53)		O13	1 ×	3.184(57)
O15	O17	2 ×	2.793(53)	O15	O7	2 ×	2.904(64)
	O7	2 ×	3.009(65)		O17	1 ×	3.056(83)
O16	O17	1 ×	3.042(48)	O16	O16	2 ×	3.089(73)
O17	O3	2 ×	3.125(70)	O17	O3	2 ×	3.008(26)
					O2	2 ×	3.099(79)

* These positions cannot be occupied simultaneously

Positron annihilation lifetime spectroscopy (PALS) results

Coincidence Doppler Broadening Spectroscopy (CDBS) is a technique to measure the Doppler broadened annihilation line (DBAL), which represents the Electron Momentum Distribution (EMD) specific for different chemical elements (Asoka-Kumar *et al.*, 1996). However, in the case of Ps formation, the DBAL contains not only EMD, but is disturbed by contributions from Ps annihilation, especially the *p*-Ps linear momentum. To correct DBAL for the presence of Ps annihilation, in order to extract EMD, it is necessary to determine the contribution from *p*-Ps (both shape and intensity). The best way is to use the PALS spectra. The *o*-Ps lifetimes and the corresponding intensities obtained by the PALS analysis are given in Table 5. Knowledge of τ_3 or τ_4 lifetimes permits determination of the average radius R as a spherical approximation of the nano-holes, where Ps is confined.

The Tao-Eldrup model was applied by setting $\tau_{o\text{-Ps}} = 0.5(1 - R/R_0 + (2\pi)^{-1}\sin(2\pi R/R_0))^{-1}$, where $\delta R = R - R_0 = 0.1656$ nm is an empirical parameter (Tao, 1972; Eldrup *et al.*, 1981). The intrinsic FWHM of the *p*-Ps linear momentum distribution, θ (approximated by a Gaussian fit) was obtained from R by another correlation $\theta = 0.424/(R + \delta R)$ keV, delivered by the same model. The intensity of the *p*-Ps was $(I_3 + I_4)/3$

TABLE 5. *o*-Ps lifetimes and the corresponding intensities obtained by PALS.

Sample	I_3 (%)	I_4 (%)	τ_3 (ns)	τ_4 (ns)	R_β (nm)	R_α (nm)
Ct	17.5±0.3	1.3±0.3	1.53±0.12	4.67±0.48	0.24±0.02	0.46±0.03
Co-c	18.2±0.4	2.1±0.5	1.53±0.15	3.67±0.42	0.24±0.02	0.40±0.03
Cp	20.4±0.4	1.3±0.4	1.49±0.12	3.91±0.42	0.23±0.02	0.42±0.03
Czn	16.9±0.3	1.3±0.2	1.55±0.11	5.60±0.43	0.24±0.02	0.50±0.02

https://doi.org/10.1180/claymin.2015.050.1.05 Published online by Cambridge University Press

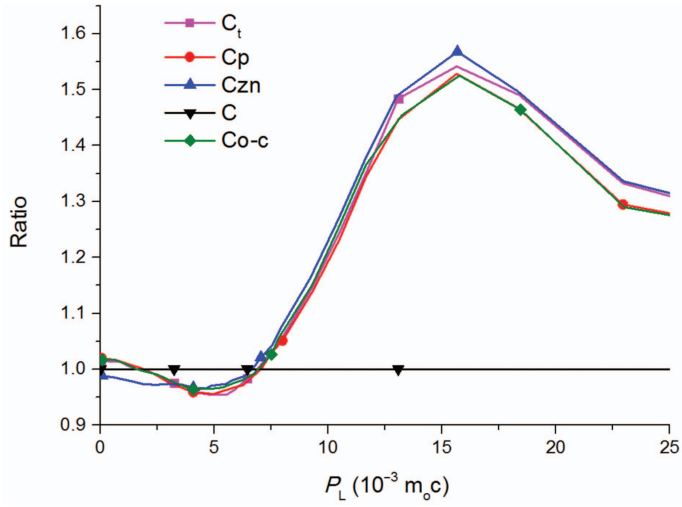

FIG. 8. EMD ratios of the studied samples over graphite

(i.e. 1/3 of the intensity of *o*-Ps). Thus, the contribution of the *p*-Ps linear momentum distribution was reconstructed using a Gaussian fit with FWHM = $(G^2 + \theta^2)^{0.5}$ and then subtracted from DBAL to obtain the value of EMD alone. A widely accepted method of enhancing the visual differences in DBALs or EMDs, is to present their ratios relative to a reference sample. Figure 8 shows the EMDs of the studied samples as ratios relative to a graphite standard. A distinct peak is observed at $\sim 16 \times 10^{-3}$ m_oc, which for the ratios relative to graphite is a fingerprint for positron annihilation with oxygen electrons (Mohamed, 2001). The framework oxygen is partly negatively charged, which makes it attractive for positrons. Hence, most of the positrons annihilate with oxygen electrons and the differences between the samples are scarcely observable. In order to check if CDBS is able to detect differences in EMDs in the samples studied the EMDs ratios relative to sample Ct are shown (Fig. 9). This representation underlined the differences between the samples, which can be classified according to similarities of EMDs into different groups. The natural clinoptilolite sample

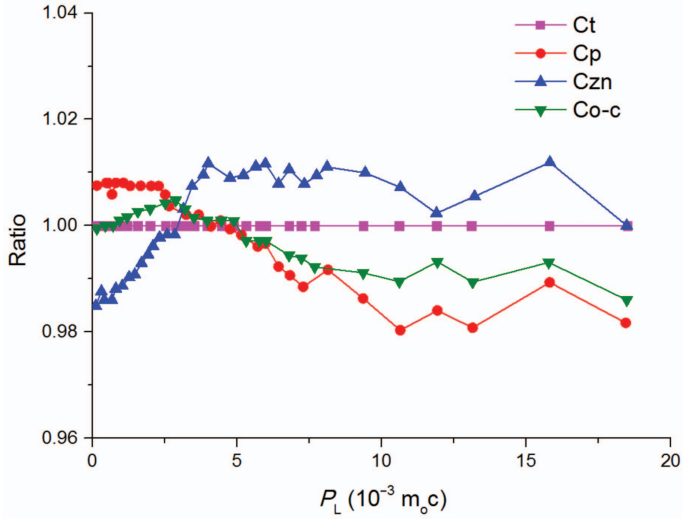

FIG. 9. EMD ratios of the studied samples over Ct.

https://doi.org/10.1180/claymin.2015.050.1.05 Published online by Cambridge University Press

(Ct), containing traces of other minerals, is different from the remaining samples. Samples Co-c and Cp show similar EMD signals. Finally, the measured EMDs of the Czn sample showed that it is sensitive to the presence of Zn. CDBS is not sensitive to the presence of opal-cristobalite and to the treatment of clinoptilolite with NaOH. However, the mineral impurities contribute to the change in EMDs, which is detectable by CDBS.

The samples show two *o*-Ps lifetimes that arise from pick-off annihilation of *o*-Ps confined in two types of pores. This finding correlates well with the clinoptilolite structure, characterized by a small β-cage (B channel) and a larger α-cage (A channel). As the PALS measurements were performed in air one has to consider the possible quenching and inhibition effect of the molecular oxygen, which has paramagnetic properties, on *o*-Ps lifetime and intensity (Mohamed, 2001). Consequently, the pore sizes given in Table 5 are a little underestimated. However, within error, the size of the β-cage is the same for all of the samples (see Table 5), i.e. the β-cage is not disturbed by the different chemical treatments or the presence of different elements (cations) in the structure. In contrast, the samples containing Zn show a larger α-cage compared to the remaining samples.

CONCLUSIONS

A method is demonstrated for obtaining an almost pure clinoptilolite sample from a zeolitized sedimentary rock. This clinoptilolite was Zn^{2+}-exchanged and the structure of this modified clinoptilolite was refined by the Rietveld method. The Zn^{2+} cations were located in three sites (Zn1, Zn2 and Zn3) within the clinoptilolite channels. Site Zn1 is in the centre of channel A, site Zn2 is in channel B, near the calcium M2 position a new Zn3 site located in channel A, very close to Zn1. Positron Annihilation Lifetime Spectroscopy (PALS) was employed to assess the Zn exchange. Since the cation content influences the free volume of the channels, the ion exchange process can be monitored by PALS. The PALS results suggest the existence of two sizes of channels, in accordance with the structural refinement data.

REFERENCES

Alietti A., Brigatti M.F. & Poppi L. (1975) Il comportammento termodifferenziale e termoponderale dei minerali del gruppo dell'heulandite. *Rendiconti della Societa Italiana di Mineralogia e Petrologia*, **31**, 613–630.

Asoka-Kumar P., Alatalo M., Ghosh V.J., Kruseman A.C., Nielsen B. & Lynn K.G. (1996) Increased elemental specificity of positron annihilation spectra. *Physical Review Letters*, **77**, 2097–2100.

Bertaux J., Fröhlich F. & Ildefonse P. (1998) Multicomponent analysis of FTIR spectra: quantification of amorphous and crystallized mineral phases in synthetic and natural sediments. *Journal of Sedimentary Research*, **68**, 440–447.

Boles J.R. (1972) Composition, optical properties, cell dimensions, and thermal stability of some heulandite group zeolites. *American Mineralogist*, **57**, 1463–1493.

Castaldi P., Santona L., Cozza C., Giuliano V., Abbruzzese, C., Nastro, V. & Melis P. (2005) Thermal and spectroscopic studies of zeolites exchanged with metal cations. *Journal of Molecular Structure*, **734**, 99–105.

Cerri G., de Gennaro M. Bonferoni C. & Caramella C. (2004), Zeolites in biomedical application: Zn-exchanged clinoptilolite-rich rock as active carrier for antibiotics in anti-acne topical therapy. *Applied Clay Science*, **27**, 141–150.

Colella C. (1999) Natural zeolites in environmentally friendly processes and applications. *Studies in Surface Science and Catalysis*, **125**, 641–655.

Copcia V.E., Hristodor C.M., Dunca S., Iordanova R., Bachvarova-Nedelcheva A., Forna N.C. & Sandu I. (2013) Synthesis and antibacterial properties of ZnO/clinoptilolite and TiO_2/$ZnTiO_3$/clinoptilolite powders. *Revista de Chimie – Bucharest*, **64**, 978–981.

Dimova L., Shivachev B.L. & Nikolova R.P. (2011) Single crystal structure of pure and Zn ion exchanged clinoptilolite: Comparison of low temperature and room temperature structures and Cu vs. Mo radiation. *Bulgarian Chemical Communications*, **43**, 217–224.

Dimowa L.T., Petrov S.L. & Shivachev B.L. (2013) Natural and Zn exchanged clinoptilolite: *in situ* high temperature XRD study of structural behavior and cation positions. *Bulgarian Chemical Communications*, **45**, 466–473.

Doula M., Ioannou A. & Dimirkou A. (2002) Copper adsorption and Si, Al, Ca, Mg and Na release from clinoptilolite. *Journal of Colloid and Interface Science*, **245**, 237–250.

Elaiopoulos K., Perraki Th. & Grigoropoulou E. (2008) Mineralogical study and porosimetry measurements of zeolites from Scaloma area, Thrace, Greece. *Microporous and Mesoporous Materials*, **112**, 441–449.

Eldrup M., Lightbody D. & Sherwood J.N. (1981) The temperature dependence of positron lifetimes in solid pivalic acid. *Chemical Physics*, **63**, 51–58.

https://doi.org/10.1180/claymin.2015.050.1.05 Published online by Cambridge University Press

Garcia-Basabe Y., Ruiz-Salvador A.R., Maurin G., de Menorval L.-C., Rodriguez-Iznaga I. & Gomez A. (2012) Location of extra-framework Co^{2+}, Ni^{2+}, Cu^{2+} and Zn^{2+} cations in natural and dealuminated clinoptilolite. *Microporous and Mesoporous Materials*, **155**, 233–239.

Habbema L., Koopmans B., Menke H.E., Doornweerd S. & de Boulle K. (1989) A 4 % erythromycin and zinc combination (Zineryt) versus 2% erythromycin (eryderm) in acne vulgaris: a randomized, double-blind comparative study. *British Journal of Dermatology*, **121**, 497–502.

Hernández-Ortiz M., Hernández-Padrón G., Bernal R., Cruz-Vázquez C., Vega-González M. & Castaño V.M. (2012) Nanostructured synthetic Opal-C. *Digest Journal of Nanomaterials and Biostructures*. **7**, 1297–1302.

Holland K.T., Bojar R.A., Cunliffe W.J., Cutcliffe A.G., Eady E.A., Farooq L., Farrell A.M., Gribbon E.M. & Taylor D. (1992) The effect of zinc and erythromycin on the growth of erythromycin-resistant and erythromycin-sensitive isolates of *Propionibacterium acnes*: an *in-vitro* study. *British Journal of Dermatology*, **126**, 505–509.

Hrenovic J., Milenkovic J., Goic-Barisic I. & Rajic N. (2013) Antibacterial activity of modified natural clinoptilolite against clinical isolates of *Acinetobacter baumannii*. *Microporous and Mesoporous Materials*, **169**, 148–152.

Kansy J. (1996) Microcomputer program for analysis of positron annihilation lifetime spectra *Nuclear Instruments and Methods in Physics Research* A, **374**, 235–244.

Kirov G.N. & Terziiski G. (1997) Comparative study of clinoptilolite and zeolite A as antimicrobial agents. Pp. 133–141 in: *Natural Zeolites, Sofia 1995* (G. Kirov, L. Filizova & O. Petrov, editors). Pensoft, Sofia - Moscow.

Korkuna O., Leboda R., Skubiszewska-Zieba J., Vrublevska T., Gunko V.M. & Ryczkowski J. (2006) Structural and physicochemical properties of natural zeolites: clinoptilolite and mordenite. *Microporous and Mesoporous Materials*, **87**, 243–254.

Koyama K. & Takeuchi Y. (1977) Clinoptilolite: the distribution of potassium atoms and its role in thermal stability. *Zeitschrift fur Kristallographie*, **145**, 216–239.

Ming D.W. & Mumpton F.A. (1989) Zeolites in soils. Pp. 873–911 in: *Minerals in Soil Environments*, 2nd Edn. (J.B. Dixon & S.B. Weed, editors). Soil Science Society of America.

Mohamed H.F.M. (2001) Study on the effect of atmosphere on A-type zeolite using positron annihilation lifetime technique. *Egyptian Journal of Solids*, **24**, 41–49.

Moirou A., Vaxevanidou A., Christidis G.E. & Paspaliaris I. (2000) Ion exchange of zeolite Na-Pc with Pb^{2+}, Zn^{2+} and Ni^{2+} ions. *Clays and Clay Minerals*, **48**, 563–571.

Mozgawa W. (2000) The influence of some heavy metals cations on the FTIR spectra of zeolites. *Journal of Molecular Structure*, **555**, 299–304.

Mumpton F.A. (1960) Clinoptilolite redefined. *American Mineralogist*, **45**, 351–369.

Perraki Th. & Orfanoudaki A. (2004) Mineralogical study of zeolites from Pentalofos area, Thrace, Greece. *Applied Clay Science*, **25**, 9–16.

Rietveld H.M. (1967) Line profiles of neutron powder diffraction peaks for structure refinement. *Acta Crystallographica*, **22**, 151–152.

Rietveld H.M. (1969) A profile refinement method for nuclear and magnetic structures. *Journal of Applied Crystallography*, **2**, 65–71.

Rodriguez-Fuentes G., Ruiz-Salvador A.R., Mir M., Picazo O., Quintana G. & Delgado M. (1998) Thermal and cation influence on IR vibrations of modified natural clinoptilolite. *Microporous Mesoporous Materials*, **20**, 269–281.

Rodríguez-Iznaga I., Gomez A., Rodríguez-Fuentes G., Benítez-Aguilar A. & Serrano-Ballan J. (2002) Natural clinoptilolite as an exchanger of Ni^{2+} and NH_4^+ ions under hydrothermal conditions and high ammonia concentration. *Microporous and Mesoporous Materials*, **53**, 71–80.

Tao S.J. (1972) Positronium annihilation in molecular substances. *Journal of Chemical Physics*, **56**, 5499–5510.

Topas V4.2 (2004) *General Profile and Structure Analysis Software for Powder Diffraction Data*, Bruker AXS Ltd.

Van Petegem S., Van Waeyenberge B., Segers D. & Dauwe C. (2003) A high-performance, high-resolution positron annihilation coincidence Doppler broadening spectrometer. *Nuclear Instruments and Methods in Physics Research, A*, **513**, 622–630.